

Pivotal Role of Water in the Mechanism of P450BM-3[†]

Donovan C. Haines, Diana R. Tomchick, Mischa Machius, and Julian A. Peterson*

Department of Biochemistry, The University of Texas Southwestern Medical Center at Dallas, Dallas, Texas 75390-9038

Received June 11, 2001; Revised Manuscript Received August 23, 2001

ABSTRACT: Cytochrome P450s constitute a superfamily of enzymes that catalyze the oxidation of a vast number of structurally and chemically diverse hydrophobic substrates. Herein, we describe the crystal structure of a complex between the bacterial P450BM-3 and the novel substrate *N*-palmitoylglycine at a resolution of 1.65 Å, which reveals previously unrecognizable features of active site reorganization upon substrate binding. *N*-Palmitoylglycine binds with higher affinity than any other known substrate and reacts with a higher turnover number than palmitic acid but with unaltered regioselectivity along the fatty acid moiety. Substrate binding induces conformational changes in distinct regions of the enzyme including part of the I-helix adjacent to the active site. These changes cause the displacement by about 1 Å of the pivotal water molecule that ligands the heme iron, resulting in the low-spin to high-spin conversion of the iron. The water molecule is trapped close to the heme group, which allows it to partition between the iron and the new binding site. This partitioning explains the existence of a high-spin–low-spin equilibrium after substrate binding. The close proximity of the water molecule to the heme iron indicates that it may also participate in the proton-transfer cascade that leads to heterolytic bond scission of oxygen in P450BM-3.

Cytochrome P450BM-3,¹ a fatty acid monooxygenase from *Bacillus megaterium*, resembles eukaryotic P450s in primary structure and function (1, 2). This self-sufficient enzyme is a complex, multidomain protein that contains heme, FAD, and FMN bound to a single polypeptide chain (1). Various P450BM-3 constructs composed of combinations of the heme-binding domain (BMP), the FMN-binding domain, or the FAD-binding domain have been cloned and expressed in bacteria (3–9). The solubility and ease of high level expression of the holoenzyme and its functional domains make this protein a very attractive model for studying flavoprotein-reductase-utilizing class II P450s.

The greatest insights into the structure/function relationship of P450 enzymes have been gained from studies on P450cam. The availability of highly diffracting crystals of a well-behaved enzyme–substrate complex of P450cam has allowed structural characterization of mechanistic intermediates (10). Of particular importance is the identification of ordered water molecules in the active site of reduced, oxygen-bound intermediates that revealed rearrangements of the proton-transfer machinery during the course of catalysis.

Unfortunately, P450cam functions differently than the clinically important eukaryotic P450s and is therefore not a good model system for class II P450s and P450BM-3. Most notably, P450cam undergoes only a slight structural rearrangement upon reduction of the substrate-bound form, whereas P450BM-3 has been shown to require a much more substantial structural rearrangement of the substrate and, by implication, the protein itself (11).

Less information is known about the reaction mechanism in P450BM-3 due to the lack of a suitable well-behaved enzyme substrate complex that could be used to carry out similar studies as for P450cam. A crystal structure of the heme domain of P450BM-3 complexed to palmitoleic acid (BMP/PA) has been previously reported. However, the crystals did not diffract to the resolution necessary to identify with certainty the positions and important mechanistic roles of catalytic solvent molecules and had weak or missing electron density for the substrate acyl chains (12). Still, the BMP/PA structure revealed a significant conformational change upon substrate binding, which involved closure of the active site channel.

Higher-resolution structural information on P450BM-3 complexed with substrates is necessary to elucidate the role of structure in its reaction mechanism. A suitable system would provide a long-awaited tool for studying the characteristics of reaction intermediates. The structural basis for the change in spin state of the heme iron from low-spin to high-spin upon substrate binding is still poorly understood. This spin state conversion is a general feature of P450s and involves expulsion of the water molecule that forms the sixth coordination site of the heme iron (13). The observation by resonance Raman spectroscopy that during substrate saturation a small amount of the low-spin species exists in

[†] This research was supported in part by research grants GM43479 and GM50858 from the NIH. The coordinates of the structure have been deposited with the Protein Data Bank and assigned the identification code 1JPZ.

* To whom correspondence should be addressed. E-mail: Julian.Peterson@email.swmed.edu; Ph: 214-648-2361; Fax: 214-648-8856.

¹ THC, tetrahydrocannabinol; GC/MS, gas chromatography/mass spectrometry; BMP, the heme domain of P450BM-3; BMP/PA, complex of the heme domain of P450BM-3 with palmitoleic acid; BMP/NPG, complex of the heme domain of P450BM-3 with *N*-palmitoylglycine; BSTFA/TMCS, *N,O*-bis(trimethylsilyl)trifluoroacetamide with 1% (v/v) trimethylchlorosilane; KPi, potassium phosphate; TMS, tetramethylsilane; PEG-3350, poly(ethylene glycol)-3350; MES, 4-morpholinethanesulfonic acid; rmsd, root-mean-square deviation.

equilibrium with the high-spin form has not been adequately explained (14). Furthermore, certain mutants retain as much as 40% low-spin character upon saturation with substrate (15).

To provide such a mechanistic tool, a substrate must be identified that contains the elements known to be required for high affinity binding to the enzyme. It has been shown that P450BM-3 utilizes fatty acid substrates and derivatives in which the carboxylic acid had been converted to an amide or alcohol, but fatty acid oxidation occurs at a rate 10–14 times greater than that of fatty acid alcohols or fatty acid amides (16). The corresponding alkanes or *O*-methylated fatty acids are not utilized as substrates. These observations were based on a relatively crude assay that did not distinguish between effects on substrate binding or turnover rate, yet they suggested that the carboxylate group uses two modes of interaction with the enzyme, one involving hydrogen bonding and a second involving ionic interactions. Biochemical studies revealed the importance of Arg47 in substrate binding (17, 18), and the distant (4.3 Å) interaction of its guanidinium group with palmitoleic acid carboxylate observed in the structure of BMP/PA (12) seems to provide the required polar interactions.

In recent years, several lines of evidence have led to the suggestion that long chain *N*-acyl amino acids may serve as physiologically active signaling molecules (19–22). One such example is arachidonylglycine, which is structurally related to the large class of active eicosanoids and specifically to the endocannabinoid arachidonylethanolamine (also known as anandamide). Recent work comparing arachidonylglycine to anandamide suggests that each compound has its own spectrum of distinct physiological effects (20). Just as the effects of anandamide parallel those of tetrahydrocannabinol (THC), the effects of arachidonylglycine appear to parallel those of THC acids, metabolites of THC. A closely related *N*-acylamino acid, *N*-palmitoylglycine, has been shown to modulate monoamine levels in the hippocampus (21, 22).

Because *N*-acylglycines contain the requisite hydrophobic acyl chain, hydrogen bond accepting carbonyl, and oxyanion of an efficient P450BM-3 substrate, we tested *N*-palmitoylglycine for substrate activity. In the present study, we report that *N*-palmitoylglycine is a substrate for P450BM-3 that binds more tightly and reacts with a higher maximal turnover number than any fatty acid substrate tested to date. Because of its increased solubility in aqueous solution as compared to the similarly sized fatty acids, *N*-palmitoylglycine reduces many experimental artifacts that plague studies utilizing high concentrations of substrate. These properties make *N*-palmitoylglycine an ideal tool for studies of the BMP/substrate complex. We determined the crystal structure of the BMP/*N*-palmitoylglycine (BMP/NPG) complex to a much higher resolution than obtained previously with palmitoleic acid, allowing us to recognize striking new details of the structural and spin state changes that occur upon substrate binding to the enzyme.

EXPERIMENTAL PROCEDURES

General Methods. The heme-, FMN-, and FAD-binding domains of P450BM-3 were purified as previously described (6, 9). The concentration of BMP was determined by the method of Omura and Sato (23). UV–visible spectroscopy

was performed on either a Hewlett-Packard model 8452A Diode Array spectrophotometer or a Varian Cary 100 double beam instrument.

Synthesis and Characterization of *N*-Acyl Amino Acids. *N*-Palmitoylglycine was synthesized in greater than 95% yield from the corresponding commercially available *N*-hydroxysuccinimidyl fatty acid and glycine by methods previously established for the fatty acylation of amino acids (24). The product was recrystallized from ethanol/10 mM HCl. Purity and identity were confirmed by ¹H NMR and GC-MS.

Substrate Characterization. For rate determination, a 1.0 mL solution of 100 μM substrate and 100 μM NADPH in 50 mM KPi, pH 7.4, was placed in a stirred cuvette at 37 °C. To this solution, P450BM-3 was added to 15 nM, and the progress of the reaction was monitored by the consumption of NADPH as indicated by the loss of absorbance at 340 nm. The rate of turnover was calculated using an extinction coefficient of 6220 M⁻¹ cm⁻¹ for NADPH. For measurement of *V*_{max}, the reaction was carried out at both 50 and 100 μM substrate to verify that the velocity was independent of substrate concentration.

For product determination, substrate was added to a 3.0 mL solution of 50 nM P450BM-3 in 50 mM KPi, pH 7.4, to a final concentration of 500 μM. To this solution, NADPH was added to 250 μM, and the progress of the reaction was monitored by the consumption of NADPH as indicated by the loss of absorbance at 340 nm. After five minutes, 1 M oxalic acid was added to lower the pH of the solution to pH 4. This mixture was immediately extracted with 3 × 3 mL dichloromethane. The combined organic extracts were washed with 3 × 1 mL distilled deionized water, dried with Na₂SO₄, and evaporated to dryness under argon. The residue was taken up in 50 μL of dichloromethane, silylated by the addition of 50 μL of *N,O*-bis[trimethylsilyl]trifluoroacetamide with 1% (v/v) trimethylchlorosilane (BSTFA/TMCS), and allowed to react at room temperature for 10 min to form trimethylsilyl (TMS) esters of the carboxylates and TMS ethers of the alcohols. The mixture was then subjected to GC/MS using an HP-5MS column (Hewlett-Packard, Palo Alto, CA). The eluted peaks were identified based upon the well-characterized mass spectrometry fragmentation patterns for silylated fatty acid alcohols, which readily established the position of the hydroxyl group (8, 25). Relative amounts of monohydroxylated products were calculated using the integration of the total ion current, which was dominated by fragmentation involving the TMS moiety.

For spectroscopic measurements, 800 μL of 7.5 μM BMP in 50 mM KPi, pH 7.4, was titrated with a solution of 10 mM substrate in 50 mM K₂CO₃ in a stirred 1.00 cm quartz cuvette. After addition of each aliquot of substrate, the solution was allowed to equilibrate for one minute before the UV–visible absorption spectrum was recorded. The data for the absorbance at 418 nm minus the absorbance at 394 nm (to give a maximal change in absorbance) were fitted to a dilution correcting equation for the bimolecular association reaction to obtain the dissociation constant.

Complex Formation and Crystallization. For complex formation, BMP (20 μM BMP in 50 mM KPi, pH 7.4) was titrated with 10 mM *N*-palmitoylglycine in 50 mM K₂CO₃ to 10% beyond the equivalence point. The extent of complexation was established by monitoring the changes in

Table 1: Statistics of Data Collection and Refinement

space group	$P2_1$
cell dimensions	$a = 59.19 \text{ \AA}$, $b = 148.36 \text{ \AA}$, $c = 64.13 \text{ \AA}$, $\beta = 98.82^\circ$
no. of measurements	475 668
no. of independent reflections	219 080
data range (\AA)	30.0–1.65
R_{merge} (%)	
overall	3.1
last shell (1.68–1.65 \AA)	28.4
data completeness (%)	
overall	84.2
last shell	38.3
$I/(\sigma)I$	
overall	23.1
last shell	1.9
no. of reflections used in refinement	218 743 (30.0–1.65 \AA)
no. of non-H protein atoms	7572
no. of water molecules	955
R_{work} (%)	17.7
R_{free} (%)	19.3
rmsd in bond lengths (\AA)	0.010
rmsd in bond angles ($^\circ$)	1.52
mean B value (\AA^2)	
mainchain	23.4
side chain	26.4
heme	18.7
substrate	30.6
water molecules	37.1
δ_A -coordinate error (\AA)	0.13
missing residues	A227, A228, A459–A470 B459–B470
no. of alternate conformations	12
rmsd C_α , mol A vs mol B (\AA)	0.25

the UV–visible spectrum. This solution was then concentrated in an Amicon centrprep-30 concentrator to a final concentration of 450 μM (25 mg/mL). The solution was stored in small aliquots at -80°C . Initial crystals were grown spontaneously at 4°C in hanging drop vapor diffusion experiments by mixing equal volumes of BMP/NPG stock solution and reservoir solution consisting of 18% (w/v) PEG-3350, 150 mM MgCl_2 , 100 mM MES, pH 6.0. The crystals obtained were not amenable to X-ray diffraction experiments but were useful as seed stock for subsequent microseeding. Diffraction quality crystals were obtained overnight after streak seeding of equilibrated drops containing a reduced concentration of enzyme (12.5 mg/mL) and a reduced concentration of PEG-3350 (12% (w/v)) in the reservoir. Crystals were transferred to fresh reservoir solution containing 20% glycerol as cryoprotectant and flash cooled in liquid propane and then stored in liquid nitrogen until used for data collection.

Data Collection. Diffraction data were collected from a single crystal at 110 K, using an R-axis IV imaging plate system (MSC, Houston, TX) mounted on a Rigaku RU-200 rotating anode ($\text{CuK}\alpha$) (Rigaku, Japan) operated at 100 mA and 50 kV. BMP/NPG crystallized with the symmetry of space group $P2_1$ (unit cell constants $a = 59.19 \text{ \AA}$, $b = 148.36 \text{ \AA}$, $c = 64.13 \text{ \AA}$, $\beta = 98.82^\circ$) with two molecules per asymmetric unit. All data were processed and scaled in the HKL2000 program suite (26). Intensities were converted to structure factor amplitudes and placed on an approximate absolute scale by the program TRUNCATE from the CCP4 package (27, 28). Data collection and processing statistics are summarized in Table 1.

Crystallographic Refinement. Refinement of the structure was carried out in the program package CNS 1.0 (29) with

a random 5% subset of all data set aside for an R_{free} calculation. Initial model coordinates were obtained by modifying the coordinates of BMP complexed with palmitoleic acid (PDB code 1fag) (4, 12) by removing the coordinates for the substrate. Rigid-body refinement of the model coordinates versus data between 20.0 and 2.5 \AA was conducted, followed by a cycle of standard positional and group isotropic atomic displacement parameter refinement. Inspection of electron-density maps in the program O (30) allowed a model for the substrate to be added. Subsequent cycles of standard positional and individual isotropic atomic displacement parameter refinement coupled with cycles of model rebuilding, modeling of alternate conformations, and addition of solvent molecules were carried out against all data from 30.0 to 1.65 \AA . Complete refinement statistics for the structure are listed in Table 1.

Structural Alignments. Structural comparisons revealed that only a portion of BMP moved upon substrate binding. As a result, our structural analyses were conducted using the residues comprising the P450 structural core (31) that do not undergo substantial movement on substrate binding. Molecule B (as defined in the PDB file) of *N*-palmitoylglycine-bound BMP was superimposed on molecule B of substrate-free BMP (PDB code 1BU7) (32) using the program Swiss PDB viewer (33) unless otherwise noted. Molecule B of substrate-free BMP has a more open substrate access channel than molecule A and therefore shows the largest structural differences, thus facilitating a detailed comparison. For all structural comparisons described in this paper, we superimposed residues: 37–43, 49–70, 85–100, 112–165, 268–380, 388–434, and 439–450, which represent approximately 62% of the amino acids of BMP. The RMSD for the C_α atoms for this superposition is 0.43 \AA .

RESULTS

Synthesis, Binding, and Metabolism of the New P450BM-3 Substrate *N*-Palmitoylglycine. *N*-Palmitoylglycine was made conveniently and in high yield from glycine and *N*-hydroxy-succinimidylpalmitate according to established methods (24). Association of the compound with BMP resulted in a UV–visible spectral perturbation similar to that caused by fatty acid substrates (Figure 1). The decrease in absorbance at 418 nm and increase in absorbance at 390 nm is typical for substrate binding to P450s and is indicative of a conversion of the heme iron from the low-spin state to a high-spin state (13). The conversion appears to be nearly complete upon saturation of the active site. The change in the UV–visible spectrum was utilized for the determination of the spectroscopic dissociation constant, K_d , of 262 nM for *N*-palmitoylglycine. This value is significantly lower than the K_d of fatty acid substrates, including palmitic acid (from which *N*-palmitoylglycine is derived). The dissociation constant for palmitic acid has been reported to be up to 10 μM and was found to bind with a K_d of 2 μM under the conditions used in this study. Thus, *N*-palmitoylglycine binds to BMP with about an order of magnitude increased affinity.

Addition of 15 nM P450BM-3 to a solution of 100 μM NADPH and 100 μM *N*-palmitoylglycine resulted in the rapid oxidation of NADPH to NADP. We found that extensive preequilibration of dilute solutions of enzyme with *N*-palmitoylglycine or palmitic acid resulted in partial

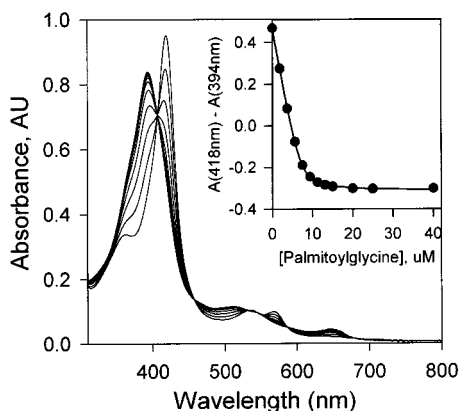


FIGURE 1: Titration of BMP with *N*-palmitoylglycine. $7.5 \mu\text{M}$ BMP in 50 mM KPi pH 7.4 was titrated with aliquots of 10 mM *N*-palmitoylglycine in 50 mM K_2CO_3 as described in Experimental Procedures. The entire UV-visible spectrum was recorded 30 s after the addition of each aliquot. Inset: Best fit of the experimental data to a model assuming a single binding site, resulting in a K_d of 262 nM.

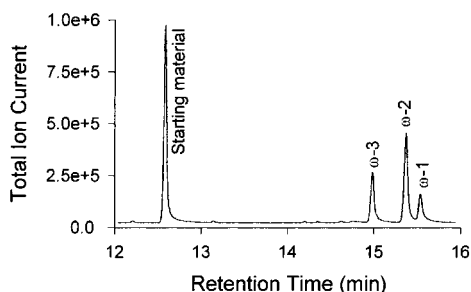
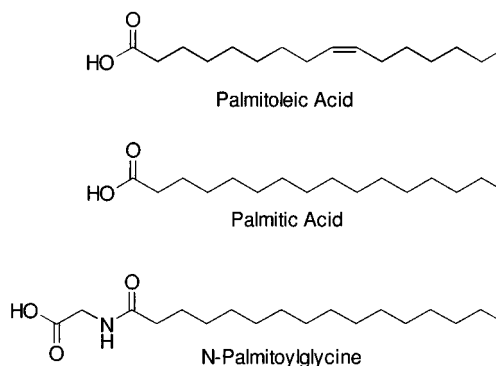


FIGURE 2: Chromatogram of P450BM-3 catalyzed products of *N*-palmitoylglycine. Product extracts with approximately 50% conversion to products were prepared and silylated with BSTFA/TMCS as described in Experimental Procedures. This solution was then injected into an HP GCD mass spectrometer containing a HP-5MS column.

inactivation of the enzyme. This may be due in part to dissociation of the FMN cofactor from the FMN-binding domain, as it has been shown that the FMN cofactor has a dissociation constant of 31 nM in aqueous solution (34). Dissociation of the FMN cofactor would also explain the observed nonlinear dependence of the maximal reaction velocity V_{max} on enzyme concentrations, which is particularly apparent at concentrations smaller than 100 nM. This complication prevents the direct comparison of turnover numbers obtained using different enzyme concentrations (35). The rate of NADPH consumption was independent of substrate concentration under the conditions used in this study and resulted in a turnover number for *N*-palmitoylglycine of $3200 \text{ mol min}^{-1} (\text{mol of enzyme})^{-1}$, 43% faster than palmitic acid under identical saturating conditions.

The enzymatic oxidation of *N*-palmitoylglycine was repeated on a larger scale and the products were extracted, silylated, and analyzed by GC-MS. The compound was converted to three major products as observed in the chromatogram (Figure 2). The products were identifiable by their mass spectra as the ω -1, ω -2, and ω -3 monohydroxylated compounds based on the well-established cleavage patterns for silylated hydroxy-fatty acids (8, 25). It has been established that P450BM-3 catalyzes the subterminal alkane hydroxylation of fatty acids, typically at these three carbons but with the major product and overall product distribution shifting

Scheme 1



slightly away from the ω -end with increasing fatty acyl chain length (8, 16, 36, 37). The distance from the carboxylate to the ω -carbon of the fatty acid moiety in *N*-palmitoylglycine is similar to that for a C19 fatty acid (Scheme 1). Consequently, one might expect the product distribution to resemble that of a C19 fatty acid. Unexpectedly, the product distribution is indistinguishable from that of palmitic acid itself under identical conditions, suggesting that the reactive end of the alkyl chain binds in a manner identical to palmitic acid.

Major Structural Changes Upon Substrate Binding. We determined a new substrate-bound structure of BMP at a higher resolution and with a lower associated coordinate error as compared to the BMP/PA complex (12), allowing a more detailed analysis of the changes that occur upon substrate binding. Statistics for the refined structure appear in Table 1.

BMP can be divided into two domains, one composed primarily of α -helices and one composed primarily of β -sheets. Two helices and a four-helix bundle form a core that is found in all P450 enzymes (38). The highly conserved Thr268, which has been shown to play an important role in catalysis (as will be discussed in detail later), is located in helix I, a component of the four-helix bundle. This residue is located near the distal face of the heme ring to one side of the iron. In all P450 structures that have been determined to high resolution, a water molecule has been identified inside the I-helix near this location. This water molecule is inserted into the normal hydrogen bond network of the helix backbone (although the exact location varies slightly from P450 to P450) at a break in the helix where the helical groove is expanded in size. This break results in a slight kink of the helix. The size and direction of the angle between the two halves varies among the different P450 enzymes.

Our structure of the BMP/NPG complex resembles the previously determined BMP/PA structure in terms of major protein conformational changes upon substrate binding. Figure 3 shows the displacement of the $\text{C}\alpha$ atoms upon binding of *N*-palmitoylglycine to BMP as compared to substrate-free BMP (molecule B of PDB entry 1BU7). The $\text{C}\alpha$ atoms of the structural core superimpose with an rmsd of 0.43 Å. The largest group of residues that differ substantially are located in the "lid domain" of the substrate access channel, which consists of the F and G helices and the loop between them. The B'-helix is in intimate contact with the G-helix and therefore moves with the lid domain. Changes in other residues are isolated and are frequently

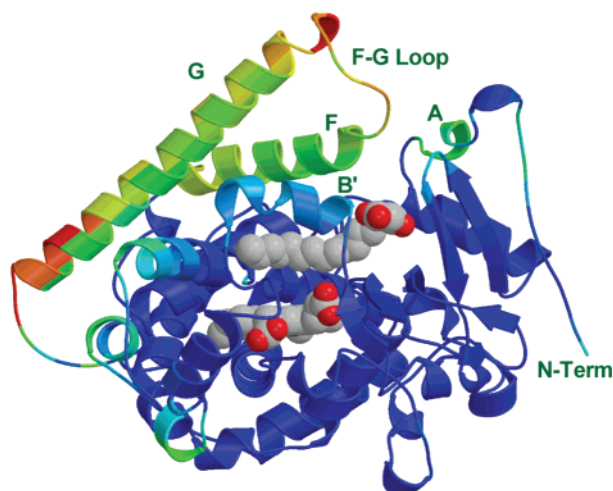


FIGURE 3: Movement of the backbone atoms upon substrate binding to BMP. The displacement of the C α atoms was converted to a color scale (dark blue corresponding to the smallest displacement and dark red corresponding to the largest displacement) and used to color the ribbon diagram. The heme is in the center of the figure and the *N*-palmitoylglycine substrate is above it; both are depicted as space-filling CPK models. This figure and Figure 6 were prepared with the programs Molscript (51) and Raster3d (47).

located in solvent-exposed turns between secondary structure elements.

BMP traps substrate molecules in the active site through a clam shell movement that involves the lid domain, the B'-helix, and the amino-terminal portion of the molecule [the "substrate-docking region" (31, 39)] (Figure 3). The lid domain exhibits a rocking motion with the I-helix as a fulcrum as well as a lateral movement toward the carboxy-terminal end of the I-helix. The substrate-docking region undergoes a complementary movement and slides toward the loop between the F and G helices. Overall, these movements appear to position the substrate molecule in the active site for the following steps in the reaction.

BMP features a large channel that extends through the entire molecule. The first portion of this channel contains the primarily hydrophobic substrate access channel and originates near the loop between the F and G helices and the substrate docking region (Figure 4A), narrows as it nears the heme iron and makes an abrupt turn perpendicular to the plane of the heme. The channel then exits on the distal face of BMP near Glu267. In the absence of substrate, the substrate access channel is filled with solvent molecules. This state is referred to as the "open" conformation (39) of BMP. In crystallographic studies, between 17 and 21 ordered water molecules have been observed in the substrate access channel, depending on the definition of its extent. It should be noted that this channel is partially blocked in monomer A in substrate-free BMP (PDB entry 1BU7), indicating that the channel exhibits pronounced plasticity.

Binding of *N*-palmitoylglycine to BMP leads to the expulsion of most solvent molecules from the central channel and the closing of the channel exit (Figure 4B). In our BMP/NPG structure, only three water molecules are present. One is near the heme iron and will be discussed in detail below. The other two water molecules are located in appendices to the substrate access channel. Substrate binding is probably driven in part by solvent effects as both desolvation of the alkyl portion of the fatty acid moiety and displacement of

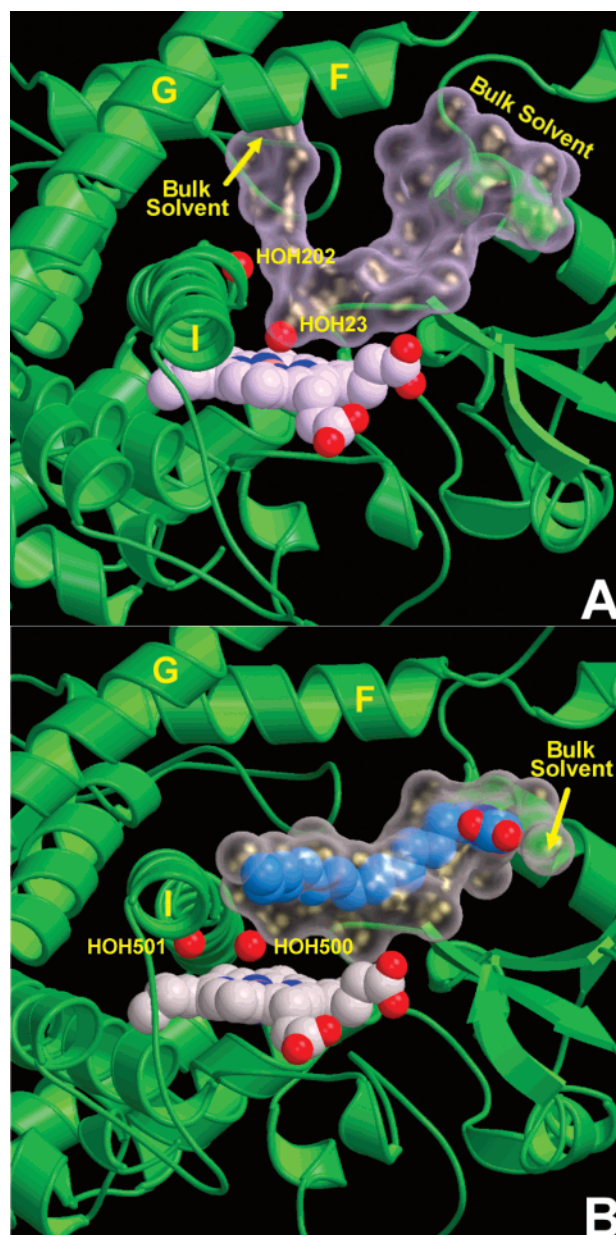


FIGURE 4: The substrate access channels of BMP, depicted as transparent surfaces. Heme, *N*-palmitoylglycine, and waters are shown in CPK space-filling representation. The channels are accessible to bulk solvent at the positions indicated. The waters shown explicitly are accessible to the substrate channels but for clarity are not covered by the transparent surfaces. These figures were prepared with the programs Molscript (51), Raster3d (52), and Grasp (53). (A) Substrate-free BMP. (B) BMP/*N*-palmitoylglycine complex; the substrate is colored light blue.

water from the central hydrophobic channel are expected to be thermodynamically favorable. Once substrate is bound, the active site region is sealed off from bulk water, which is a necessary prerequisite for efficient substrate oxidation.

Interactions between N-Palmitoylglycine and BMP. *N*-Palmitoylglycine binds to BMP in a similar fashion as palmitoleic acid. Because the hydrogen bond between Tyr51 (Figure 5) and the fatty acid carbonyl is retained in both the BMP/NPG and BMP/PA complexes, the carbon atoms of their alkyl chains are in similar positions (12). The only differences result from saturation of the double bond at C₉₋₁₀ of palmitoleic acid. As a consequence, the ω -end of the fatty acid of the *N*-palmitoylglycine molecule extends approxi-

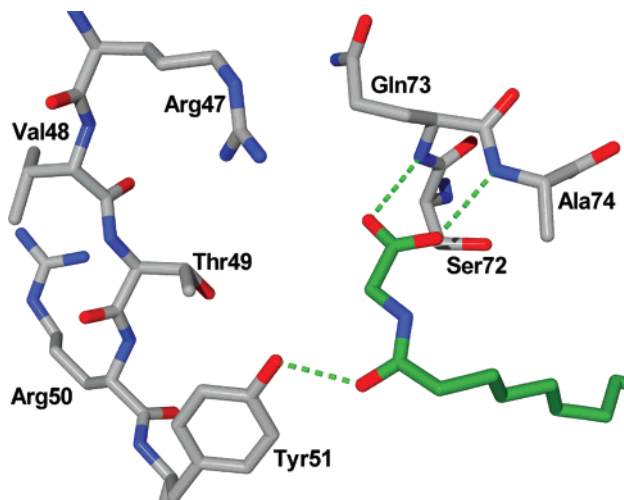


FIGURE 5: The hydrogen bond network in the carboxylate binding pocket and interactions with *N*-palmitoylglycine. Hydrogen bonds are drawn as green dashed cylinders. Carbon atoms are colored white, oxygen is red, and nitrogen is blue. This figure was prepared in the programs Swiss PDB Viewer (33) and POV Ray (<http://www.povray.org>).

mately one angstrom farther into the enzyme cleft than palmitoleic acid. The conservation of the binding mode for the alkyl portions of the substrates explains the retention of substrate specificity from palmitic acid to *N*-palmitoylglycine.

N-palmitoylglycine establishes polar interactions with the amino terminus of the B'-helix that are not present in the BMP/PA complex. The glycine carboxylate group forms two hydrogen bonds with the backbone nitrogen atoms of Gln73 and Ala74, thereby bridging the substrate access channel between Tyr51 and the B'-helix. The B'-helix is shifted by less than 0.3 Å from the position in the BMP/PA structure. The negatively charged end of the substrate is closer to the B'-helix, which allows a more favorable electrostatic interaction with the helix dipole moment. These features of *N*-palmitoylglycine likely explain its increased binding affinity.

The importance of Arg47 for substrate binding to P450BM-3 has been noted, but its exact role is unclear. In our BMP/NPG crystal structure, the Arg47 guanidinium group is 4.5 Å from the carboxyl group of the glycine moiety, similar to the BMP/PA complex where the distance to the substrate carboxyl group is about 5.2 Å (12). The difference between these distances is within the experimental error of the BMP/PA structure. As the authors note, this distance is too long for an efficient electrostatic interaction. Instead of stabilizing the bound state of the substrate, Arg47 may be important for the kinetics of the association reaction, e.g., for electrostatic steering or in transient bound states that exist as intermediates between the uncomplexed and observed complexed form. This hypothesis is supported by the fact that the charge-reversed Arg47Glu mutant results in about a 3-fold decrease in the affinity of BMP for palmitate but a 7-fold decrease in k_{cat} , although some controversy exists on these results (17, 18, 40).

Active Site Rearrangement. Substrate binding to BMP is accompanied by rearrangements of pivotal water molecules and the hydrogen bond network in the active site region. Details of this rearrangement are now recognizable due to the significantly higher resolution of our BMP/NPG structure as compared to the BMP/PA complex.

A change in the conformation of the I-helix is accompanied by changes in ordered water molecules within the helix backbone. The normal hydrogen bonding pattern of the backbone residues of the I-helix is interrupted in the substrate-free form by a water molecule that is inserted between the Ile263–Glu267 and the Ala264–Thr268 carbonyl oxygens and backbone amides. The helix has a 13° kink centered on this interruption. When substrate is bound this water molecule is absent, permitting the formation of the Ile263–Glu 267 hydrogen bond. A water molecule (WAT501) is present in a new position (Figure 6) that retains the interactions with the Ala264 carbonyl and now hydrogen bonds to the Thr269 side chain and amide NH. One result of this rearrangement is that the I-helix in the substrate-bound form now deviates only 5° from linearity.

This rearrangement in the I-helix causes the displacement of the water molecule that fills the sixth coordination site of the heme iron. The structural changes in the I-helix result in a 1.7 Å shift of the Ala264 carbonyl away from the heme iron (Figure 6). This shift allows the heme water ligand (WAT500) to shift concurrently and interact with the side chain of Thr268 resulting in an essentially planar hydrogen bond network involving the two water molecules, the carbonyl oxygen of Ala264, and the Thr268 hydroxyl. As a result, WAT500 is located above and displaced in a direction parallel to the heme plane and off to the side of the iron, where oxygen will bind upon reduction. The close proximity of this ordered water molecule to the oxygen binding site suggests it will play a vital role in later mechanistic steps.

DISCUSSION

The results presented herein establish the BMP/NPG complex as a powerful tool for the study of cytochrome P450 mechanism. The primary model system for P450 structure and mechanism has been P450cam; however, the structural changes accompanying substrate binding and catalysis in P450cam are not representative of those occurring in P450BM-3 and the clinically important eukaryotic class II P450s. The novel high-affinity P450BM-3 substrate *N*-palmitoylglycine, with its favorable biochemical properties, now opens new avenues for investigating structure and mechanism of the more complex class II P450s.

Our structural study of BMP/NPG provides extensive insight into the function of P450BM-3. First, it reveals that substrate binding effects a change in heme iron spin state and closes a solvent-accessible channel via a protein conformational change that behaves as a molecular switch. Second, the existence of the water molecule near the heme iron in the substrate bound form provides an explanation for observed variations in the low-spin high-spin equilibrium in the substrate bound state. Finally, the localization of this water at the site where oxygen will bind after enzyme reduction provides the clearest picture to date of the proton donors required for scission of dioxygen.

A Substrate-Binding Induced Molecular Switch. The changes in protein structure between the free and substrate bound states can be described as a molecular switch that has clear functional significance beyond substrate recognition. The changes greatly reduce solvent access to the enzyme active site, alter heme iron reduction potential via a change in heme iron ligation, and leave the sixth coordination site of the heme iron available for molecular oxygen.

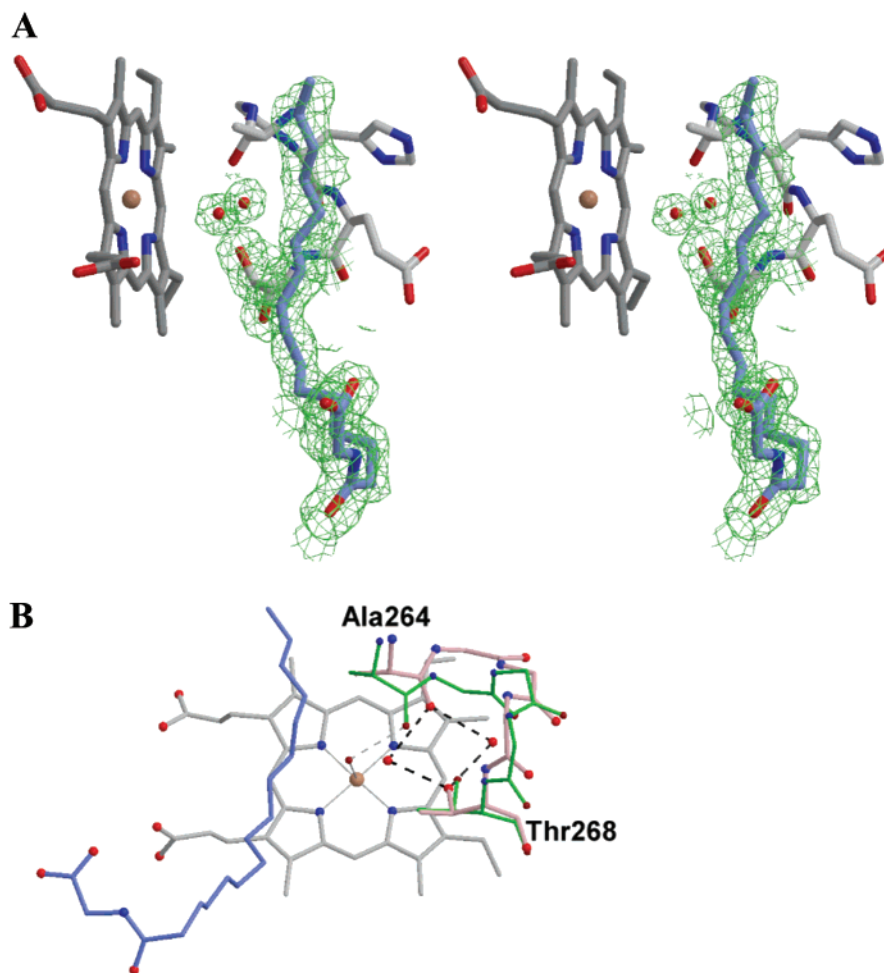


FIGURE 6: (A) Simulated annealing $2F_o - F_c$ omit map (contoured at 1σ) in the region of WAT500 and WAT501. (B) Water binding sites in the substrate cavity superimposed to residues 264 to 268 of the substrate-free and BMP/NPG complex. Shown in pink is a stick model for the BMP/NPG complex, in green is the substrate-free complex, in gray is the heme, and in blue is the *N*-palmitoylglycine substrate. Hydrogen bonds for the BMP/NPG complex are drawn as black dashed lines, and for the substrate-free in gray. Side chains for residues 265 to 267 were removed for clarity. Oxygen atoms are colored red, nitrogen atoms are blue and iron atoms are brown.

Destabilizing steric interactions with protein or substrate do not drive the displacement of WAT500 from the heme iron. Examination of the structure reveals that the substrate does not approach closely enough to the water molecule to displace it directly. Only the atoms of the Phe87 side chain approach the ligand site closely enough to interfere with the heme iron–water interaction. In the Phe87Ala mutant, where this phenyl ring has been removed and cannot displace the water molecule, the heme efficiently undergoes a nearly complete low-spin to high-spin conversion comparable to wild-type enzyme upon saturation with lauric acid (41) or *N*-palmitoylglycine (our laboratory, unpublished results). The lack of destabilizing interactions suggests the formation of a higher affinity site for the water molecule.

Examination of the substrate bound structure supports a mechanism where substrate binding provides the driving force for a protein rearrangement that causes the generation of the high affinity WAT500 binding site. Prior to substrate binding, this water molecule is stabilized by the ligand interaction with the heme iron and a hydrogen bond to Ala264. After substrate binds and the resulting rearrangement in the I-helix causes Ala264 to withdraw away from the heme iron, the water would only have the ligand interaction to hold it in place. We will refer to this binding site as the “L-site”, due to the heme iron’s low-spin nature

in this arrangement. A new water binding site, the “H-site” (the heme iron is 5-coordinate and high-spin in this arrangement), is formed nearby that is stabilized by hydrogen bonds to Ala264 and Thr268. The L-site and H-site are too close together to both contain water molecules simultaneously, so WAT500 preferentially occupies the higher affinity H-site leaving the lower affinity L-site empty as observed in the BMP/NPG structure.

The net effect is that of a molecular switch, where substrate binding converts the enzyme from a form with low catalytic competence to a form with high catalytic competence. The protein rearrangement restricts the access of bulk solvent to the active site, opens the sixth coordination site of the heme iron so that oxygen can bind after enzyme reduction, and changes the heme iron to high-spin. Restricting solvent access to the site where the active oxidant will be generated is important in protecting it from undesirable side reactions. The change to high-spin lowers the reduction potential, making the heme iron easier to reduce. This modulation of reduction potential has been postulated to provide a partial “gating” mechanism that increases the efficiency of usage of reducing equivalents by preventing the reduction of enzyme that is not catalytically competent due to the lack of bound substrate (31). Overall, the changes prepare the enzyme for later steps in catalysis.

Competition between WAT500 Binding Sites Determines the Low-Spin:High-Spin Equilibrium in the Substrate Bound State. Our structure of BMP complexed to *N*-palmitoylglycine explains certain enigmatic observations of the spin state distribution in some forms of the enzyme. Resonance Raman studies of P450BM-3 have demonstrated that in the presence of saturating concentrations of substrate, an equilibrium exists between the five-coordinate, high-spin and the six-coordinate, low-spin states (14). Varying small amounts of low-spin heme iron, depending on the fatty acid substrate used, are present even in the absence of any detectable substrate dissociation or photoreduction. In the Thr268Ala mutant of P450BM-3, about 40% of the enzyme remains in the low-spin state when complexed to arachidonic acid (15). These results can now be simply explained by an equilibrium existing between the L- and H-sites, such that in the wild type enzyme the H-site is not exclusively populated but does heavily predominate. The two sites cannot be populated simultaneously due to their close proximity to each other and no structural barrier exists that would prevent a water molecule from making the short transition from one site to the other. In the Thr268Ala mutant, the additional hydrogen bond is not available to stabilize the water molecule at the H-site, thus the equilibrium is shifted toward the L-site.

The dependence of the relative affinities of the two sites on the exact position of Ala264 and the structure of the I-helix provides a potential structural coupling from the active site to the surface of the enzyme. It has already been observed that the position of the surface exposed carboxy-terminus of the I-helix changes position simultaneously with the change in position of Ala264 during the binding of substrate. Resonance Raman studies on both the isolated heme domain and the heme domain still fused to the reductase (FMN) domain have shown that, in the substrate-bound state of P450BM-3, the presence of the FMN domain increases the fraction of the six coordinate, low-spin state of the heme iron (14). The FMN domain binds to the loop region (Gly240–Asp250) that immediately precedes the I-helix in P450BM-3 (32). It was proposed that an increase in solvent accessibility of the heme-binding pocket caused by the presence of the FMN domain could account for the change in the spin state equilibrium. Instead, because our structural data suggest that the spin state equilibrium is determined by the partitioning of the central water molecule between the L- and H-sites, binding of the FMN-domain may in fact indirectly destabilize the H-site. This destabilization could be due to a structural coupling between the FMN-binding site and the H-site transmitted through the I-helix.

Proton Transfer during Dioxigen Scission. The rearrangement of water molecules near the heme iron upon substrate binding provides new insights into the mechanism of O–O bond scission. P450 enzymes produce a powerful electron deficient ferryl oxidant by heterolytic cleavage of the O–O bond in the two-electron-reduced oxygen-bound enzyme (42). The accompanying buildup of negative charge on the distal oxygen atom has to be stabilized. One of the proposed mechanisms for the charge stabilization is the donation of two protons. It has been suggested that these protons could be delivered through a proton-transfer cascade from bulk solvent to the oxygen via the side chain of Thr268 (43).

This threonine is well conserved in P450 enzymes and has been shown to play an important role in the catalytic

mechanism (15, 44). Experiments on the equivalent residue in P450cam have established that coupling (efficient use of electrons for substrate hydroxylation without generation of reactive oxygen species) requires the hydrogen bond accepting side chain oxygen (43). Coupling does not require the exchangeable proton at the threonine side chain position, and catalytic activity is affected by but not strictly dependent on its presence (45). Similar effects have been observed for the conserved threonine (Thr268) in P450BM-3. Mutation of Thr268 to alanine reduces the rate of lauric (44) and arachidonic acid (15) oxidation. Concomitant with the decrease in substrate hydroxylation rate is a loss of coupling efficiency [16% coupling for lauric acid oxidation (44), 9% for arachidonic acid oxidation (15)].

The importance of ordered water molecules and hydrogen bonding networks in the active site of P450s is underscored by studies on P450eryf. Although P450eryf lacks the threonine that forms part of the binding site for both WAT500 and WAT501 in the BMP/NPG structure, it features two active site waters in equivalent positions as observed in the structure of P450eryf in complex with its natural substrate 6-deoxyerythronolide B (PDB code 1OXA) (46, 47). Structural and kinetic analyses show that the role of the side chain of Thr268 in BMP is taken over in P450eryf by a substrate hydroxyl group, resulting in exquisite substrate specificity (47, 48). Introduction of an active site threonine into P450eryf through mutagenesis confers the ability to oxidize many alternate substrates (49). Also, mutants that perturb the solvent structure in the active site decrease the catalytic activity of P450eryf and increase uncoupling (50).

Consistent with the studies on P450eryf and P450cam, our structure reveals that the role of the conserved threonine is primarily to interact with water molecules near the oxygen binding site in P450BM-3. In the oxidized substrate bound structure, the H-site is stabilized by interaction with this side chain. Although no determination can be made as to which is the hydrogen bond donor and which is the acceptor from the structural data, if P450BM-3 is active in the absence of the exchangeable threonine proton as in P450cam the threonine is most likely the acceptor. The 1.7 Å movement of the axial water ligand upon binding of substrate does not allow room for molecular oxygen to bind to the heme iron. The water molecule must either be displaced by molecular oxygen (or by CO in CO bound reduced enzyme) or it must move beyond the van der Waals radius of the liganded oxygen atom for catalysis to proceed.

An examination of reaction intermediate structures for P450cam sheds light on the possible role of this water-binding site in proton donation during catalysis for P450 enzymes (10). The structures of BMP/NPG and the reduced, oxygen- and substrate-bound P450cam are nearly identical in the vicinity of the conserved threonine side chain even though they differ substantially in their substrate-free forms. In P450cam, two water molecules are observed in the one-electron reduced, oxygen bound structure that were not seen in structures of earlier reaction pathway intermediates. One of these water molecules (WAT902) is located in the I-helix in a position very similar to the BMP/NPG WAT501. The other (WAT901) is located within hydrogen bonding distance to the carbonyl of Gly248 (the equivalent of Ala264 in BMP) and the side chain of the conserved Thr252 similar to BMP/NPG WAT500 but is displaced away from the heme relative

to the WAT500. The distal atom of heme bound dioxygen occupies the BMP/NPG WAT500 site and is within hydrogen bonding distance of WAT901. This water is proposed to play a role in proton donation to the dioxygen. In the subsequent P450cam reaction pathway intermediate, where a second electron was added and oxygen bond scission occurred, a water molecule is seen near the distal oxygen atom site in a position now nearly identical to that of WAT500 in BMP/NPG. In this post-scission structure, ordered water molecules are no longer observed in the WAT901 and WAT902 sites. Examination of the BMP/NPG structure reveals that there is a vacant cleft in the region analogous to the WAT901 site of P450cam that is large enough to accommodate a movement of WAT500 upon binding of oxygen. These structural similarities suggest that the active oxidant is generated by the same mechanism in BMP as in P450cam.

The possible interaction between WAT500 (or WAT901) and the heme bound dioxygen could serve to promote the heterolytic cleavage of the O—O bond. The potential hydrogen bond that this water could donate to the distal oxygen atom would serve to stabilize the buildup of negative charge. One clear role for this water molecule would be the donation of at least one of the two requisite protons to the distal oxygen. This may be an important feature in the generation of the extremely electron deficient oxidant generated in P450 enzymes. Finally, the ability of the enzyme to sequester the product water molecule in the WAT500 binding site as observed for WAT902 in P450cam would be an important step in protecting the highly active oxidant once it is formed.

The structural features of the BMP/NPG complex presented herein reveal important insights into the early steps of catalysis in P450s. We expect the BMP/NPG complex to be a valuable tool for studying later steps, e.g., the nature of the mechanistic intermediate that actually carries out scission of dioxygen. Upon anaerobic reduction, our BMP/NPG crystals crack. This observation is consistent with a conformational change occurring upon reduction, as implicated by NMR studies and the unreasonably long Fe—substrate distances in the two substrate complex structures (11, 12). Attempts to crystallize the complex under anaerobic conditions are underway, as are attempts to cocrystallize the BMP/NPG complex with the FMN-binding domain.

REFERENCES

- Narhi, L. O., and Fulco, A. J. (1987) *J. Biol. Chem.* 262, 6683–90.
- Ruettinger, R. T., Wen, L. P., and Fulco, A. J. (1989) *J. Biol. Chem.* 264, 10987–95.
- Narhi, L. O., Wen, L. P., and Fulco, A. J. (1988) *Mol. Cell. Biochem.* 79, 63–71.
- Li, H. Y., Darwish, K., and Poulos, T. L. (1991) *J. Biol. Chem.* 266, 11909–14.
- Oster, T., Boddupalli, S. S., and Peterson, J. A. (1991) *J. Biol. Chem.* 266, 22718–25.
- Sevrioukova, I., Truan, G., and Peterson, J. A. (1996) *Biochemistry* 35, 7528–35.
- Govindaraj, S., and Poulos, T. L. (1997) *J. Biol. Chem.* 272, 7915–21.
- Sevrioukova, I., Truan, G., and Peterson, J. A. (1997) *Arch. Biochem. Biophys.* 340, 231–8.
- Boddupalli, S. S., Oster, T., Estabrook, R. W., and Peterson, J. A. (1992) *J. Biol. Chem.* 267, 10375–80.
- Schlichting, I., Berendzen, J., Chu, K., Stock, A. M., Maves, S. A., Benson, D. E., Sweet, R. M., Ringe, D., Petsko, G. A., and Sligar, S. G. (2000) *Science* 287, 1615–22.
- Modi, S., Sutcliffe, M. J., Primrose, W. U., Lian, L.-Y., and Roberts, G. K. (1996) *Nat. Struct. Biol.* 3, 414–7.
- Li, H., and Poulos, T. L. (1997) *Nat. Struct. Biol.* 4, 140–6.
- Peterson, J. A. (1971) *Arch. Biochem. Biophys.* 144, 678–93.
- Deng, T. J., Proniewicz, L. M., Kincaid, J. R., Yeom, H., Macdonald, I. D., and Sligar, S. G. (1999) *Biochemistry* 38, 13699–706.
- Truan, G., and Peterson, J. A. (1998) *Arch. Biochem. Biophys.* 349, 53–64.
- Miura, Y., and Fulco, A. J. (1975) *Biochim. Biophys. Acta* 388, 305–17.
- Graham-Lorence, S., Truan, G., Peterson, J. A., Falck, J. R., Wei, S., Helvig, C., and Capdevila, J. H. (1997) *J. Biol. Chem.* 272, 1127–35.
- Oliver, C. F., Modi, S., Primrose, W. U., Lian, L. Y., and Roberts, G. C. (1997) *Biochem. J.* 327, 537–44.
- Burstein, S. H. (2000) *Curr. Pharm. Des.* 6, 1339–45.
- Burstein, S. H., Rossetti, R. G., Yagen, B., and Zurier, R. B. (2000) *Prostaglandins Other Lipid Mediat.* 61, 29–41.
- Vamvakides, A. (1995) *Boll. Chim. Farm.* 134, 258–62.
- Vamvakides, A. (1994) *Boll. Chim. Farm.* 133, 369–73.
- Omura, T., and Sato, R. (1964) *J. Biol. Chem.* 239, 2370–8.
- Lapidot, Y., Rappoport, S., and Wolman, Y. (1967) *J. Lipid Res.* 8, 142–145.
- Marinetti, G. V. (1976) *Lipid Chromatographic Analysis*, 2nd rev. and expand ed.; M. Dekker, New York.
- Otwinowski, Z., and Minor, W. (1997) *Methods Enzymol.* 276, 307–26.
- French, S., and Wilson, K. (1978) *Acta Crystallogr. A* 34, 517–25.
- Project, C. C. (1994) *Acta Crystallogr. D* 50, 760–3.
- Brünger, A. T., Adams, P. D., Clore, G. M., DeLano, W. L., Gros, P., Grosse-Kunstleve, R. W., Jiang, J. S., Kuszewski, J., Nilges, M., Pannu, N. S., Read, R. J., Rice, L. M., Simonson, T., and Warren, G. L. (1998) *Acta Crystallogr. D* 54, 905–21.
- Jones, T. A., Zou, J. Y., Cowan, S. W., and Kjeldgaard. (1991) *Acta Crystallogr. A* 47, 110–9.
- Hasemann, C. A., Kurumbail, R. G., Boddupalli, S. S., Peterson, J. A., and Deisenhofer, J. (1995) *Structure* 3, 41–62.
- Sevrioukova, I. F., Li, H., Zhang, H., Peterson, J. A., and Poulos, T. L. (1999) *Proc. Natl. Acad. Sci. U.S.A.* 96, 1863–8.
- Guex, N., and Peitsch, M. C. (1997) *Electrophoresis* 18, 2714–23.
- Haines, D. C., Sevrioukova, I. F., and Peterson, J. A. (2000) *Biochemistry* 39, 9419–29.
- Matson, R. S., Hare, R. S., and Fulco, A. J. (1977) *Biochim. Biophys. Acta* 487, 487–494.
- Boddupalli, S. S., Estabrook, R. W., and Peterson, J. A. (1990) *J. Biol. Chem.* 265, 4233–9.
- Capdevila, J. H., Wei, S., Helvig, C., Falck, J. R., Belosludtsev, Y., Truan, G., Graham-Lorence, S. E., and Peterson, J. A. (1996) *J. Biol. Chem.* 271, 22663–71.
- Graham, S. E., and Peterson, J. A. (1999) *Arch. Biochem. Biophys.* 369, 24–9.
- Ravichandran, K. G., Boddupalli, S. S., Hasemann, C. A., Peterson, J. A., and Deisenhofer, J. (1993) *Science* 261, 731–6.
- Li, H., and Poulos, T. L. (1999) *Biochim. Biophys. Acta* 1441, 141–9.
- Oliver, C. F., Modi, S., Sutcliffe, M. J., Primrose, W. U., Lian, L. Y., and Roberts, G. C. (1997) *Biochemistry* 36, 1567–72.

42. Groves, J. T., and Han, Y. (1995) In *Cytochrome P450: Structure, Mechanism, and Biochemistry* (Ortiz de Montellano, P. R., Ed.) pp 3–48, Plenum, New York.
43. Imai, M., Shimada, H., Watanabe, Y., Matsushima-Hibiya, Y., Makino, R., Koga, H., Horiuchi, T., and Ishimura, Y. (1989) *Proc. Natl. Acad. Sci. U.S.A.* 86, 7823–7.
44. Yeom, H., Sligar, S. G., Li, H., Poulos, T. L., and Fulco, A. J. (1995) *Biochemistry* 34, 14733–40.
45. Kimata, Y., Shimada, H., Hirose, T., and Ishimura, Y. (1995) *Biochem. Biophys. Res. Commun.* 208, 96–102.
46. Cupp-Vickery, J. R., Li, H., and Poulos, T. L. (1994) *Proteins* 20, 197–201.
47. Cupp-Vickery, J. R., and Poulos, T. L. (1995) *Nat. Struct. Biol.* 2, 144–53.
48. Cupp-Vickery, J. R., Han, O., Hutchinson, C. R., and Poulos, T. L. (1996) *Nat. Struct. Biol.* 3, 632–7.
49. Xiang, H., Tschirret-Guth, R. A., and Ortiz De Montellano, P. R. (2000) *J. Biol. Chem.* 275, 35999–6006.
50. Choonkeun, K., Haeyoung, K., and Oksoo, H. (2000) *Bioorg. Chem.* 28, 306–14.
51. Kraulis, P. J. (1991) *J. Appl. Crystallogr.* 24, 946–50.
52. Merritt, E. A., and Bacon, D. J. (1997) *Methods Enzymol.* 277, 505–24.
53. Nicholls, A., Sharp, K. A., and Honig, B. (1991) *Proteins* 11, 281–96.

BI011197Q